Proceedings of the 1993
ASME Winter Meeting
New Orleans, LA Dec. 1993

NASA-TM-112086

STUDIES OF GAS-LIQUID FLOW IN MICROGRAVITY: VOID FRACTION, PRESSURE DROP AND FLOW PATTERNS

W.S. Bousman
Department of Chemical Engineering
University of Houston
Houston, Texas

A.E. Dukler
Department of Chemical Engineering
University of Houston
Houston, Texas

ABSTRACT

A 1.27 cm diameter two phase gas-liquid flow experiment has been developed with the NASA Lewis Research Center to study two-phase flows in microgravity. The experiment allows for the measurement of void fraction, pressure drop, film thickness and bubble and wave velocities as well as for high speed photography. Three liquids were used to study the effects of liquid viscosity and surface tension, and flow pattern maps are presented for each. The experimental results are used to develop mechanistically based models to predict void fraction, bubble velocity, pressure drop and flow pattern transitions in microgravity.

INTRODUCTION

Two phase gas-liquid flows are expected to occur in a wide variety of future space operations including [1]:

Design and operation of the space station thermal management system

Storage and transfer of cryogenic fluids

Control of two phase power cycles

Safety and performance issues concerning space nuclear power systems

With the lack of buoyancy in the microgravity environment, two phase gas-liquid flows are expected to behave differently from those in earth gravity. In order to reliably design two phase equipment for the microgravity environment, models are needed to predict quantities such as flow pattern transitions, pressure drop and void fraction. Physically based models will have the widest range of applicability but experimental data will be needed to develop and verify these models.

EXPERIMENTAL APPARATUS

A microgravity two phase flow experiment has been developed in conjunction with the NASA Lewis Research Center (LeRC). This experiment is flown in the LeRC Learjet in parabolic trajectories to produce periods of microgravity (0 ± 0.02 g) lasting up to 20 seconds. During this period, two phase mixtures are introduced into an instrumented test section. The system is controlled by a computer which also provides for data acquisition and storage.

The flow loop used on board the aircraft is shown in Figure 1. This system provides metered quantities of air and liquid to the mixer. Air is fed axially into a 1.27 cm ID mixing section while liquid is introduced into the sides of the tube through a series of small holes. The resulting two phase mixture flows into a 1.27 cm ID development section which provides 86 pipe diameters of flow development length. The two phase mixture then enters the test section. The mixture from the test section passes through several layers of screens in a collection tank. Surface tension retains the liquid for later reuse while the gas passes through under a pressure driving force.

The test section used in the experiments is shown in Figure 2. The section allows for simultaneous measurement of liquid film thickness, void fraction and pressure drop, all at 1000 Hz, while also allowing for high speed photography of the flow. Film thickness and void fraction are measured using parallel wire conductance probes. The void fraction probe consists of two 0.076 mm diameter Pt-Rh wires spaced 2.5 mm apart and spanning the cross section of the tube. The film thickness probe is identical to the void fraction probe except that half of the length of each wire is insulated with a thin coating of spray rubber so that the film thickness is measured on only one side of the tube. The velocity of bubbles, slugs or waves can be determined by cross correlating the signals from the two probes positioned along the axis. These probes are operated by a high speed conductance measurement system developed at the University of Houston which outputs a voltage proportional to the conductance between the wires. The

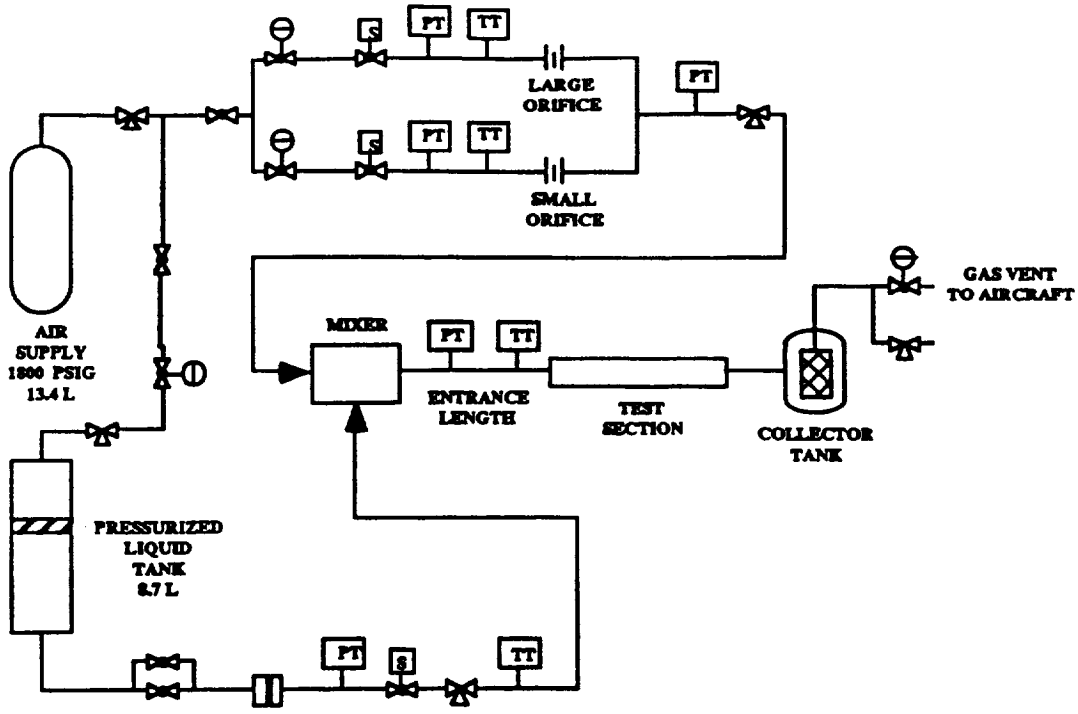

FIGURE 1
NASA LERC LEARJET TWO PHASE FLOW LOOP

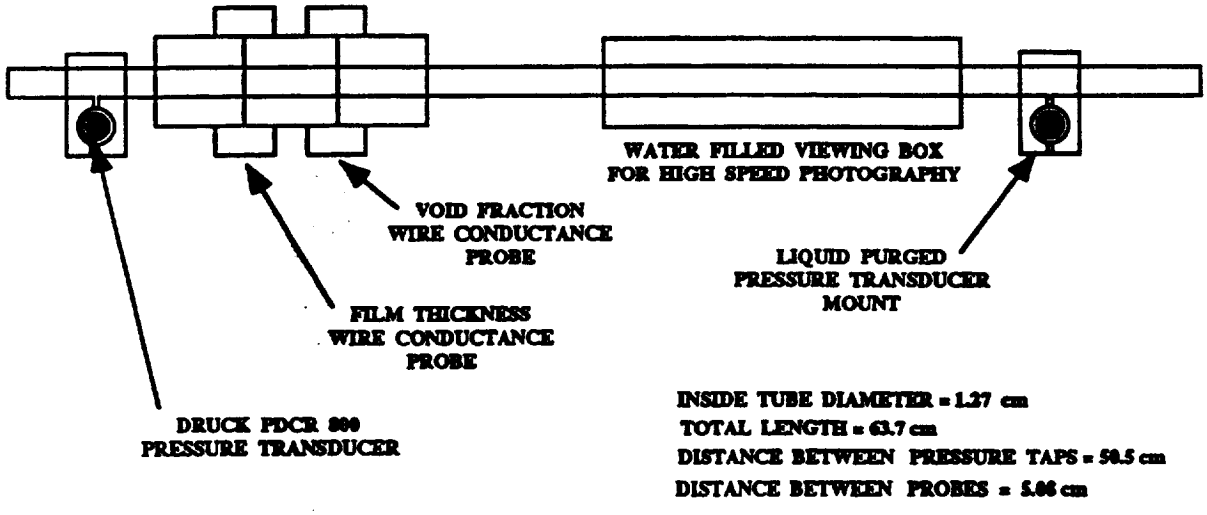

FIGURE 2
1.27 CM ID TEST SECTION

conductance is related to the local thickness of the fluid. The probes are calibrated to relate the output voltage to film thickness or void fraction. Conductivity of the liquid is measured continuously during a run using a standard cell so that changes in the specific conductance of the fluid or the fluid temperature do not affect the results. The typical response time for the probes to a step change is less than 500 μs.

Pressure drop is measured using two Druck PDRC 820 flush mounted pressure transducers which are spaced 0.5 m apart in the test section. These fit into liquid filled cavities which are connected to the test section through a small channel. Prior to the experiment, the taps are purged with the same liquid used in the experiment to remove air bubbles from the taps. The purge is turned off during the experiment and observations have shown that the taps remain free of bubbles during the reduced gravity runs. The resulting pressure signals are electronically subtracted to provide differential pressure. The accuracy of the transducers is better than 1%.

To visualize the flow patterns, the flow is photographed at 400 frame/sec using a high speed movie camera. The viewing section of the tube is surrounded by a water filled box which reduces refraction effects at the plexiglass-air interface. The viewing box is backlit to provide sharp contrast between the air and liquid.

Three liquids were used to test the effect of physical properties: water (μ_L = 1.0 cP, σ_L = 72 dyne/cm), 50-50 wt% water-glycerine (μ_L = 6.0 cP, σ_L = 63 dyne/cm) and water with 0.5 wt% Dupont Zonyl FSP Fluorosurfactant (μ_L = 1.0 cP, σ_L = 20 dyne/cm). These liquids were made conductive for the film thickness and void fraction measurements by the addition of a small amount of NaCl.

FLOW PATTERN MAPS

For any one pipe size, two phase flows distribute themselves into several distinct flow patterns depending primarily on the liquid and gas flowrates in the system and the fluid properties. Determining the nature of these flow patterns as well as their locations across the parameter space is important because models which are specific to a single flow pattern are usually more successful than global models spanning the entire space.

Over the course of several years, the authors have performed a large number of microgravity experiments over a large range of the liquid and gas flowrate parameter space with the three liquids described above. As shown in Figure 3, three distinct flow patterns have been observed in microgravity [2]. The bubbly flow pattern is characterized by gas bubbles distributed in a continuous liquid phase. In slug flow, most of the gas is found in bullet shaped Taylor bubbles which alternate with bubbly liquid slugs. Annular flow consists of a wavy liquid film on the tube wall surrounding a core of gas. In addition, transitional states between bubbly and slug flow and slug and annular flow have been observed. Flows in transition exhibit features of both of the adjacent flow patterns.

Flow pattern identification was accomplished both using film thickness traces and the movie films. Flows were considered to be bubbly when the gas bubbles had a length less than the diameter of the tube. At the bubble-slug transition, small Taylor bubbles were present along with masses of smaller bubbles. Slug flows were identified from film thickness traces which clearly resolve the Taylor bubbles and

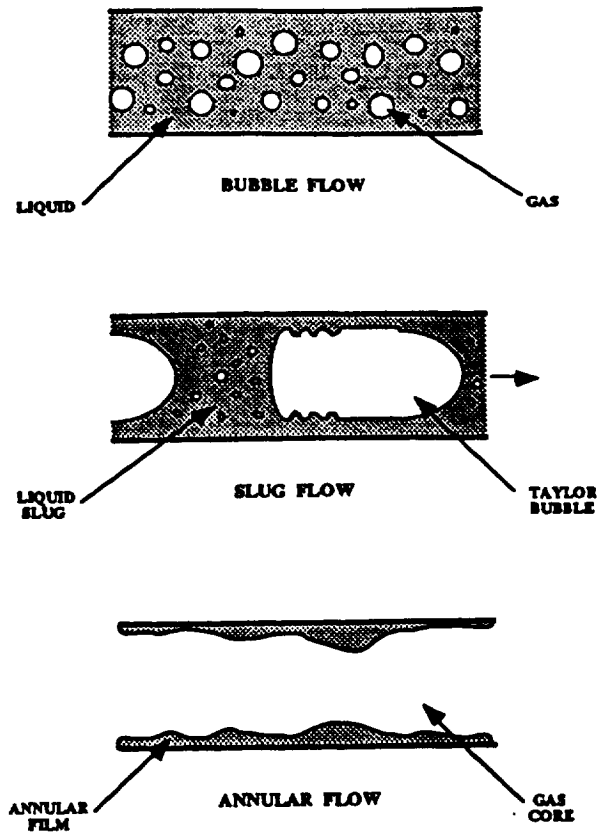

FIGURE 3
FLOW PATTERNS OBSERVED IN MICROGRAVITY

liquid slugs. Flows were considered to be annular when the waves on the liquid film did not bridge the pipe as determined by film thickness and photography. The region of slug-annular transition is one in which annular waves briefly bridge the pipe to form liquid slugs then unbridge again. Since the waves travel at velocities greater than 1 m/s and the bridging events are short lived, identifying the slug-annular transition region is difficult.

The identification of the flow pattern as a function of liquid and gas superficial velocity is shown for each liquid in Figures 4, 5 and 6. It can be seen that there is a shift in the location of the bubble-slug transition between the water and water-Zonyl FSP maps and a shift in the slug-annular transition between the water and water-glycerine maps.

VOID FRACTION

The analysis by Zuber and Findlay [3] demonstrates that the radial distribution of the void fraction and velocities in two phase flows are not, in general, uniform, yet the measurements taken usually represents an average over the cross section rather than a local value. This can be accounted for if the models are developed using cross sectional average quantities defined as:

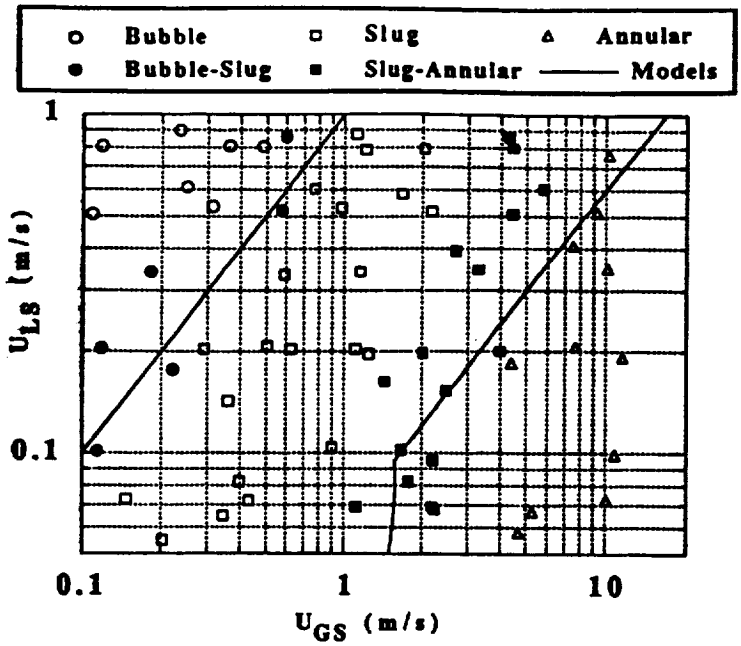

FIGURE 4
MICROGRAVITY FLOW PATTERN MAP FOR 1.27 CM ID TUBE, AIR-WATER

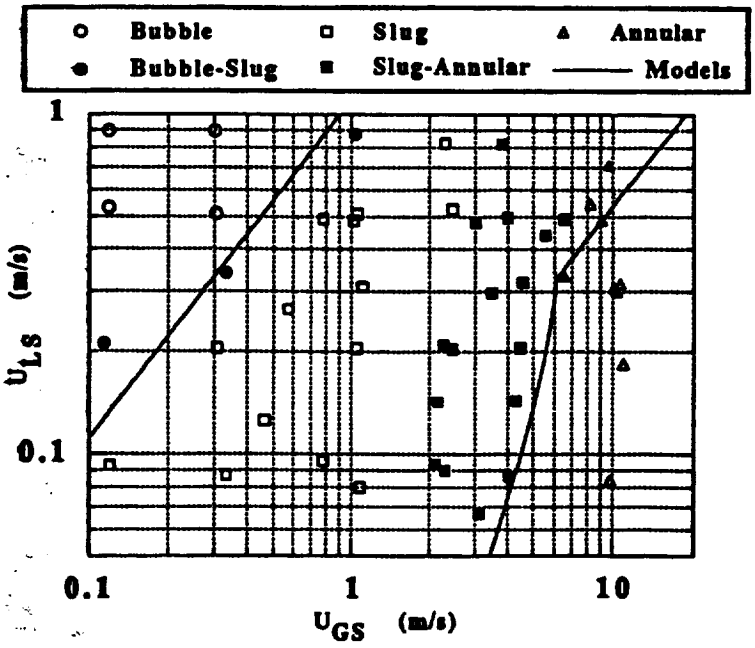

FIGURE 5
MICROGRAVITY FLOW PATTERN MAP FOR 1.27 CM ID TUBE, AIR-WATER/GLYCERINE

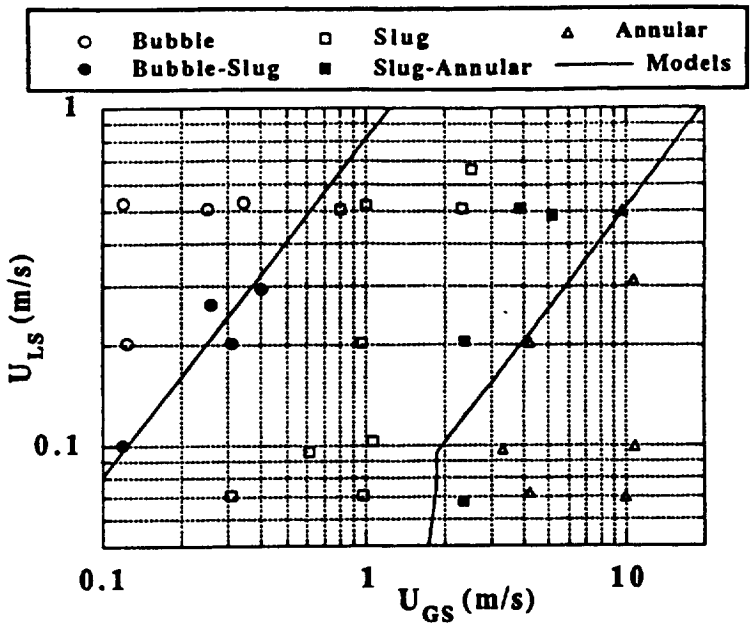

FIGURE 6
MICROGRAVITY FLOW PATTERN MAP FOR 1.27 CM ID TUBE, AIR-WATER/ZONYL

$$\langle F \rangle = \frac{1}{A}\int_A F dA \quad (1)$$

where F is any local quantity varying with radial position and A is the cross sectional area of the test section.

The average superficial velocities of gas and liquid can be related to the average velocity and void fraction , $\langle\alpha\rangle$, by:

$$U_{GS} = \langle\alpha\rangle\langle U_G\rangle \quad (2)$$

$$U_{LS} = (1-\langle\alpha\rangle)\langle U_L\rangle \quad (3)$$

while the total is defined as:

$$U_{MS} = U_{GS} + U_{LS} \quad (4)$$

U_M is the local volumetric flux of liquid plus gas at any radial position while U_{MS} is the cross sectional average. This is of course the sum of the superficial velocities.

From a mass balance, the average gas velocity can be expressed as:

$$\langle U_G\rangle = \frac{\langle\alpha U_M\rangle}{\langle\alpha\rangle} + \frac{\langle\alpha V_G\rangle}{\langle\alpha\rangle} \quad (5)$$

where $\langle V_G\rangle$ is the average net drift velocity of the gas with respect to $\langle U_M\rangle$. This drift should not be present in microgravity due to the lack of buoyancy between the liquid and gas. Observations of the movie films of bubble and slug flows confirm that the drift velocity is negligible in the microgravity experiments and the second term in (5) can be neglected.

To account for non-uniform distribution of the void fraction over the cross sectional area, Zuber and Findlay [3] define the distribution coefficient C_o as:

$$C_o = \frac{\langle\alpha U_M\rangle}{\langle\alpha\rangle U_{MS}} \quad (6)$$

Equation (6) indicates that for a uniform distribution of voids and velocity, $C_o = 1$. Zuber and Findlay [3] show that if the concentration of voids is greater at the centerline than at the wall, $C_o > 1$, attaining a value of 1.5 for a parabolic distribution of void fraction and velocity.

By combining (2), (5) and (6), the relation between void fraction and superficial velocities is obtained:

$$\frac{U_{GS}}{U_{MS}} = C_o\langle\alpha\rangle \quad (7)$$

To test the validity of (7), the left hand side is plotted against the time average of the measured void fraction for each fluid in Figures 7, 8 and 9. This is possible because the void fraction measured by the two wire conductance probe is a cross

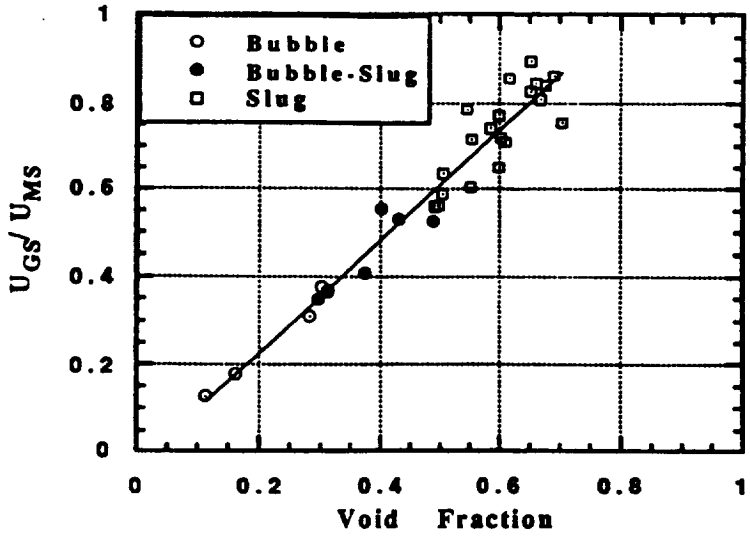

FIGURE 7
RELATION BETWEEN VOID FRACTION AND SUPERFICIAL VELOCITIES
FOR 1.27 CM ID TUBE, AIR-WATER

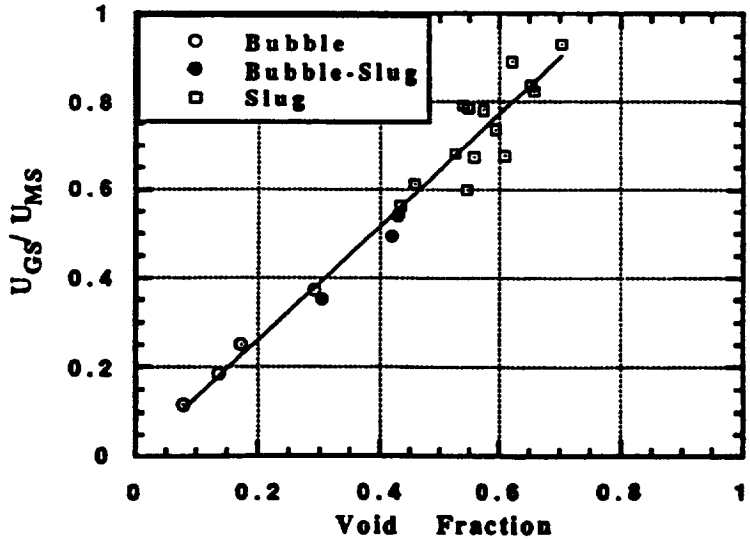

FIGURE 8
RELATION BETWEEN VOID FRACTION AND SUPERFICIAL VELOCITIES
FOR 1.27 CM ID TUBE, AIR-WATER/GLYCERINE

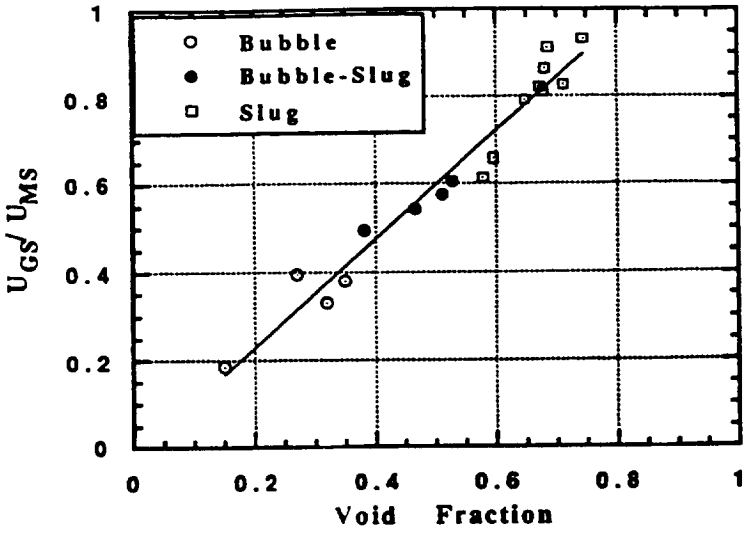

FIGURE 9
RELATION BETWEEN VOID FRACTION AND SUPERFICIAL VELOCITIES
FOR 1.27 CM ID TUBE, AIR-WATER/ZONYL FSP

sectional average quantity. As shown, the plots are linear with an intercept of 0 ± 0.03 for all three liquids. The zero intercept confirms the assumption of a negligible drift velocity. The distribution coefficient determined from the slope of each curve fit is $C_o = 1.25$ for water, $C_o = 1.28$ for water/glycerine and $C_o = 1.24$ for water/Zonyl FSP, which indicates that the concentration of voids is greater at the centerline than at the wall since $C_o > 1$. This is qualitatively confirmed by the movie films as well.

The difference between the measured void fraction and that predicted by (7) was computed for each fluid. Since the slug runs in Figures 7 and 8 show more scatter than the bubble flow runs, the error was also computed for the individual flow patterns. The error in prediction for each is reported in Table 1. On average, equation (7) predicted the measured void fraction to within 5%.

A model for predicting $\langle U_G \rangle$, the cross sectional average velocity of the bubbles in bubble and slug flow, is obtained by combining (2) and (7) to yield:

$$\frac{\langle U_G \rangle}{U_{MS}} = C_o \qquad (8)$$

Experimental values of $\langle U_G \rangle$ were obtained from cross correlation of the void fraction and film thickness traces and used to test equation (8). The results are plotted in Figures 10, 11 and 12 for each of the three liquids. The values of C_o obtained from the slopes in these figures are 1.35, 1.47 and 1.31 for water, water/glycerine and water/Zonyl FSP respectively. The discrepancy between these values of C_o and those computed using equation (7) is attributed to experimental error in the determination of $\langle U_G \rangle$. The error in determining the time lag used to compute the velocity is estimated at 13% for $\langle U_G \rangle = 1.5$ m/s due to limitations in the resolution of the cross correlation.

TABLE 1.
ERROR IN VOID FRACTION PREDICTED BY (7)

LIQUID	FLOW PATTERN	MEAN DEV.	STD. DEV.
Water	Bubble	0.017	0.012
	Slug	0.009	0.048
	All	0.012	0.042
Water/Gly.	Bubble	-0.011	0.010
	Slug	-0.007	0.050
	All	-0.003	0.042
Water/Zonyl	Bubble	0.010	0.046
	Slug	0.012	0.042
	All	0.014	0.038

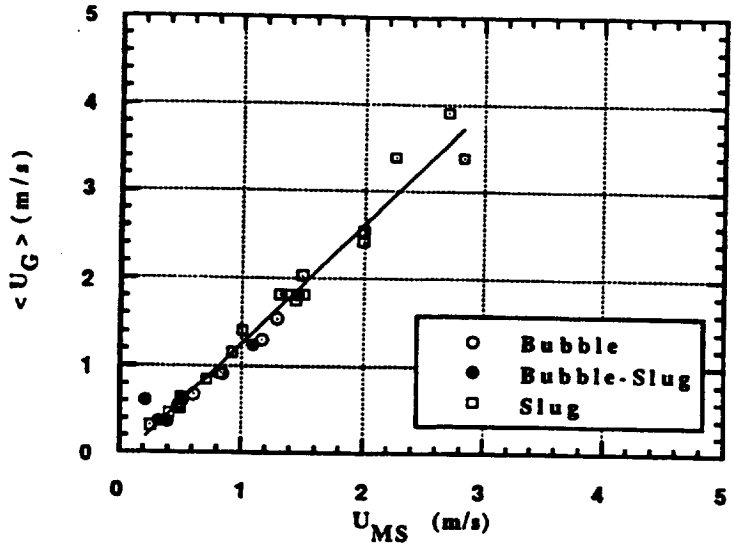

FIGURE 10
VELOCITY RELATIONSHIP FOR AIR-WATER

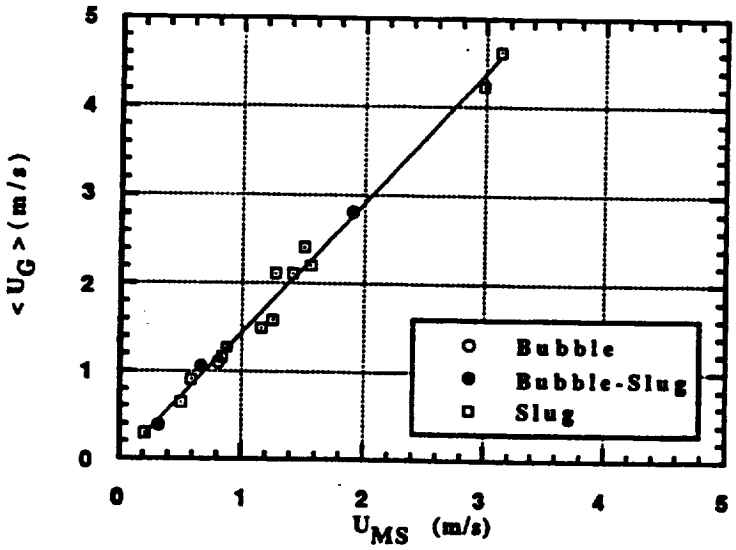

FIGURE 11
VELOCITY RELATIONSHIP FOR AIR-WATER/GLYCERINE

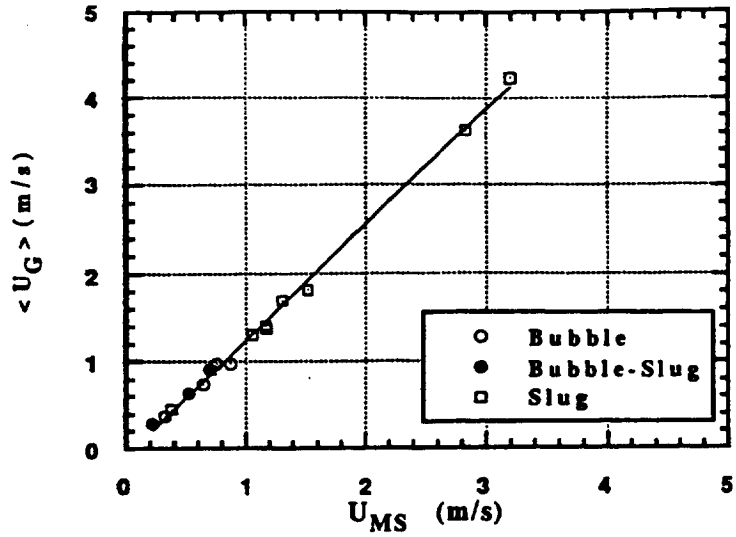

FIGURE 12
VELOCITY RELATIONSHIP FOR AIR-WATER/ZONYL FSP

The overall result of this analysis is that once a value of C_o is established, Equation (7) provides a model for predicting the average void fraction from superficial velocities. Equation (8) provides a model for predicting the velocity of bubbles and slugs from superficial velocities. Furthermore, the value of C_o gives insight into the nature of the radial distribution of the voids.

PRESSURE DROP

Bubble Flow

Because bubble flow can be perceived as a homogeneous mixture of liquid and gas, a possible approach to modeling the pressure drop would be to use the Fanning equation using the mixture velocity and density. The pressure drop for bubble flow would be expressed as:

$$\frac{dP}{dx} = \frac{2 f_{TP} \rho_M U_{MS}^2}{D} \qquad (9)$$

where U_{MS} is given by (4), f_{TP} is the two phase friction factor, D is the test section diameter, and the mixture density ρ_M is defined in terms of the liquid and gas densities, ρ_L and ρ_G, by:

$$\rho_M = <\alpha> \rho_G + (1-<\alpha>) \rho_L \qquad (10)$$

Similarly the Reynolds number for bubbly flow is defined as

$$Re_{TP} = \frac{D \rho_M U_{MS}}{\mu_L} \qquad (11)$$

The viscosity of the liquid, μ_L, is used rather than that of the mixture because the wall region is essentially gas free.

For comparison, the friction factor for a perfectly smooth tube is given by the Blasius relation:

$$f = \frac{C}{Re^n} \qquad (12)$$

with C = 16 and n = 1 for laminar flow and C = 0.046 and n = 0.2 for turbulent flow.

Friction factors for the microgravity bubble flow runs were computed using the time averaged differential pressure measurements and are plotted versus Reynolds number in Figure 13. The plot shows that bubble flow runs for the 1.27 cm ID pipe lie mostly in the laminar-turbulent transition region, which makes modeling difficult.

The microgravity two phase friction factors shown in Figure 13 lie 30% to 50% above the Blasius friction factor curves. Since deviations from perfect smoothness in the test section such as pipe roughness, flanges etc. could cause this

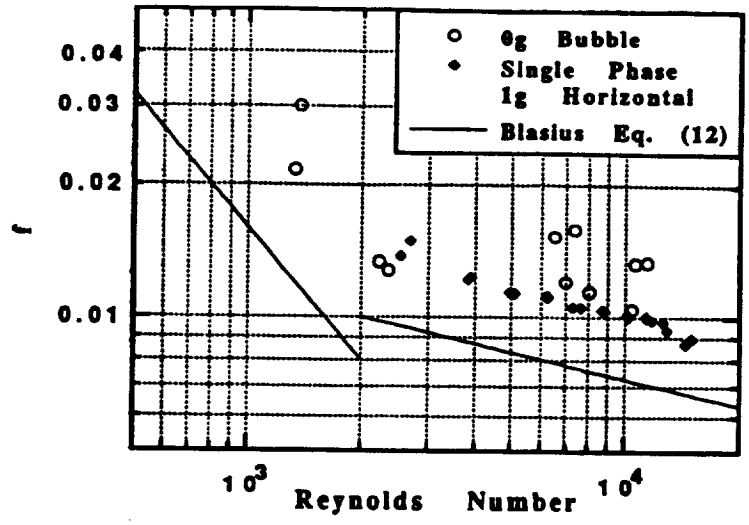

FIGURE 13
FRICTION FACTORS FOR MICROGRAVITY BUBBLE FLOW, 1.27 CM ID TUBE

discrepancy, single phase liquid flow experiments were used to provide a control. These results, plotted in Figure 13, also show a 30% increase in friction factor as compared to the Blasius relation but show much less scatter than the bubble flow runs. This tends to suggest that two phase microgravity friction factors can be computed from single phase correlations if the appropriate density and velocity are used, although more experiments are needed to verify this.

Slug Flow

It is of interest to determine if the homogeneous model applies to slug and bubble slug transition flows. These results are plotted with the bubble and single phase results in Figure 14. As shown, the slug flow runs exhibit a large amount of scatter about the single phase values. The bubble-slug transition runs as well as the slug flow runs located near the transition on the flowmaps exhibit a distinct increase in friction factor over the other slug flow runs which is presently unexplained.

Annular Flow

The interfacial friction factor, f_i, can be computed from the measured pressure gradient, dP/dx, and the effective diameter for gas flow, D - 2 h, as follows:

$$f_i = \frac{(D - 2\bar{h})}{2\rho_G \langle U_G \rangle^2} \left|\frac{dP}{dx}\right| \qquad (13)$$

where $\bar{h}$ is the time average film thickness.

Using (2) to express the gas velocity in terms of superficial gas velocity and noting that the average void fraction in annular flow is related to the average film thickness by:

$$\langle \alpha \rangle = \left(1 - \frac{2\bar{h}}{D}\right)^2 \qquad (14)$$

leads to:

$$f_i = \frac{\langle \alpha \rangle^{3/2} D}{2\rho_G U_{GS}^2} \left|\frac{dP}{dx}\right| \qquad (15)$$

The friction factor can be cast into the form of an enhancement of the single phase gas flow friction factor by dividing by the Blasius relation (12) for the gas alone:

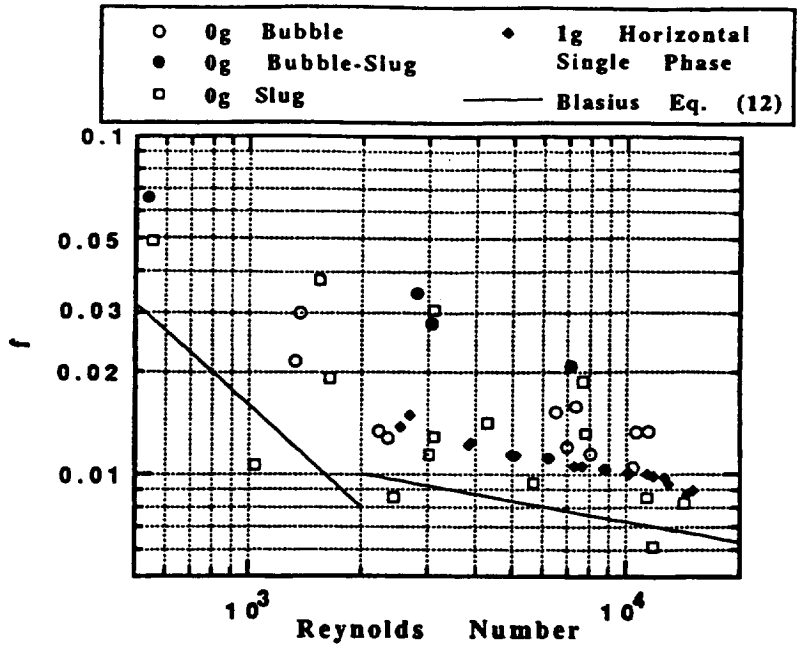

FIGURE 14
FRICTION FACTORS FOR MICROGRAVITY TWO PHASE FLOW, 1.27 CM ID TUBE

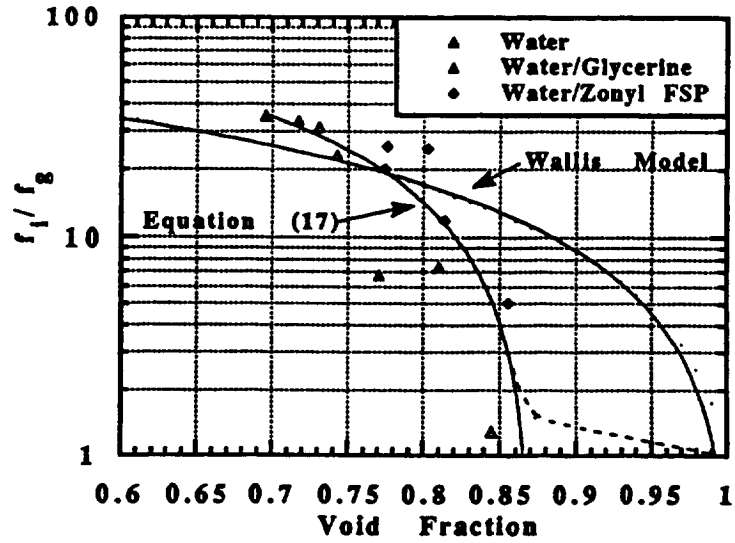

FIGURE 15
MICROGRAVITY ANNULAR FLOW FRICTION FACTOR ENHANCEMENT, 1.27 CM ID TUBE

$$\phi = \frac{f_i}{f_G} = \frac{\frac{<\alpha>^{3/2} D}{2 \rho_G U_{GS}^2}\left|\frac{dP}{dx}\right|}{\left(\frac{C}{Re_G^n}\right)} \quad (16)$$

where Re_G is the Reynolds number calculated for the gas alone with a channel diameter corrected for the presence of the liquid film.

The friction factor enhancement ϕ, calculated from the measured void fraction and pressure drop, is plotted against void fraction for all three liquids in Figure 15 for a limited number of annular and slug-annular transition runs for which pressure drop data was available. The annular flow runs exhibit a linear trend for $0.7 < <\alpha> < 0.85$ which can be fit by

$$\phi = \frac{f_i}{f_G} = 211.4 - 245.9 <\alpha> \quad (17)$$

and is shown in Figure 15.

This simple model does not yield the correct result in the limit of $<\alpha> = 1$ where the friction factor ratio should become unity. The friction factor enhancement appears to be only slightly affected by the presence of the liquid film for void fractions exceeding $<\alpha> = 0.85$. A model which does behave properly in this limit is the model proposed by Wallis [4] for 1g annular flow friction factor:

$$\frac{f_i}{f_G} = 1 + 150(1 - <\alpha>^{0.5}) \quad (18)$$

This model is also shown in Figure 15. Clearly there is a large discrepancy between the Wallis model and the experimental annular flow data. This may be resolved with the additional microgravity annular flow experiments which are now underway.

BUBBLE-SLUG TRANSITION MODEL

A simple mechanism for the transition from bubbly to slug flow assumes that the transition occurs when the bubble density is sufficient for the bubbles to encounter each other and coalesce. Such a mechanism would imply that the transition occurs at a distinct value of void fraction. The void fraction measurements shown in Figures 7,8 and 9, show that the runs identified as being at the bubble-slug transition lie in a range of void fractions separating the bubbly and slug flow runs. The transitional runs lie in the range of $0.3 \le \alpha \le 0.49$ for water, $0.3 \le <\alpha> \le 0.43$ for water-glycerine and $0.38 \le <\alpha> \le 0.53$ for water-Zonyl FSP experiments, suggesting that the transition mechanism is affected by the surface tension of the liquid. The range of transition void fractions reported may be broadened somewhat by the use of photography to identify the flow patterns since bubble or slug flow runs exhibiting even a short period of the other flow pattern were designated as transition runs.

Another constraint on the void fraction of bubbly flow comes from the maximum packing density of bubbles before they must touch and coalesce. It can be shown that this upper limit is $<\alpha> = 0.52$, independent of bubble diameter. The maximum value of 0.53 noted for the water-Zonyl FSP runs is consistent with this limit within the experimental error of the void fraction measurement. While this provides an upper limit, Figures 7 and 8 clearly show that slug flow can exist for $<\alpha> \le 0.52$. This is likely due to contacts between bubble caused by turbulence and deformation of the bubbles.

To develop the transition model, equation (3) is substituted into (7) and solved for U_{LS}:

$$U_{LS} = \frac{(1 - C_o <\alpha>)}{C_o <\alpha>} U_{GS} \quad (19)$$

To utilize this model, the void fraction at the center of the transition zone was used, yielding $<\alpha>_w = 0.40$ for water, $<\alpha>_w = 0.37$ for water-glycerine and $<\alpha>_w = 0.45$ for water-Zonyl FSP. The value of C_o used for each liquid were those computed from Figures 7,8 and 9 using equation (7). Substituting these results into (19) leads to the bubble-slug transition model for each liquid:

water: $U_{LS} = 1.0\, U_{GS}$ (20)

water/glycerine: $U_{LS} = 1.11\, U_{GS}$ (21)

water/Zonyl FSP: $U_{LS} = 0.792\, U_{GS}$ (22)

These models are plotted in Figures 4, 5 and 6 and clearly separate the bubble and slug flow regions of the flowmaps. The results suggest that the presence of the Zonyl FSP surfactant retards the coalescence of the bubbles, leading to bubble flow at higher values of void fraction than would be observed with water alone. The difference between the water and water/glycerine results are due primarily to differences in the distribution coefficient, indicating that the distribution of the voids may also play a role in the rate at which bubbles encounter each other and coalesce.

SLUG-ANNULAR TRANSITION MODEL

Photographic observations of flows near the transition of slug and annular flow indicate that as the void fraction of slug flow increases, a point is reached where the liquid slugs become short enough to rupture. At this point the flow becomes annular. Similarly, as the void fraction of an annular flow decreases, the amplitude of the waves increases until the waves bridge the pipe, creating a liquid slug. These observations suggest that the transition should occur when slug and annular models predict the same void fraction, as suggested by Dukler et. al. [1].

A force balance on the annular flow leads to:

$$\tau_i = \tau_w <\alpha>^{1/2} \quad (23)$$

where τ_i and τ_w represent the shear stress at the gas-liquid interface and at the wall respectively. These can be expressed in terms of friction factors by:

$$\tau_i = f_i \frac{\rho_G <U_G>^2}{2} = f_i \frac{\rho_G U_{GS}^2}{2 <\alpha>^2} \quad (24)$$

$$\tau_w = f_w \frac{\rho_L < U_L >^2}{2} = f_w \frac{\rho_L U_{LS}^2}{2(1-<\alpha>)^2} \quad (25)$$

Substituting (24) and (25) into (23) leads to:

$$\frac{<\alpha>^{3/2}}{(1-<\alpha>)^2} = \frac{f_i}{f_w} \frac{\rho_G}{\rho_L} \left(\frac{U_{GS}}{U_{LS}}\right)^2 \quad (26)$$

This force balance was checked for annular and slug-annular transition runs as follows. The void fraction <α> was available from experimental data. The interfacial friction factor f_i was computed from measured pressure drop data and <α> using (15). The wall friction factor f_w was computed from (12) using appropriate values of C and n depending on the magnitude of the liquid Reynolds number. Agreement was achieved to within 20% for all experiments with much better agreement attained for the runs at the lower void fractions.

All that remains is to develop suitable expressions for the friction factors. Assuming that the interfacial friction factor can be expressed as an enhancement of the single phase gas friction factor which is a function of the void fraction yields:

$$f_i = \phi f_G \quad (27)$$

and friction factors for the liquid and the gas flowing alone are given by the Blasius relation (12). The appropriate single phase Reynolds numbers are:

$$Re_G = \frac{D U_{GS} \rho_G}{\mu_G <\alpha>^{1/2}} \quad (28)$$

$$Re_L = \frac{D U_{LS} \rho_L}{\mu_L} \quad (29)$$

Using the constants in the Blasius relation for turbulent gas and liquid flow, and substituting (27), (28) and (29) into (26) results in the annular flow relation:

$$U_{LS} = U_{GS} \left[\frac{(1-<\alpha>)^2}{B <\alpha>^{2.4}} \phi\right]^{0.556} \quad (30)$$

where

$$B = \left(\frac{\nu_L}{\nu_G}\right)^{0.2} \left(\frac{\rho_L}{\rho_G}\right) \quad (31)$$

The value of B is 481.5 for water and water-Zonyl FSP and 759.8 for water-glycerine.

Similarly, the relation for laminar liquid flow and turbulent gas flow becomes:

$$U_{LS} = \frac{0.00288\ D^{0.8} \nu_G^{0.2} \rho_G U_{GS}^{1.8} (1-<\alpha>)^2 \phi}{\mu_L <\alpha>^{2.4}} \quad (32)$$

To impose the void fraction matching constraint, equations (30) or (32) are equated with the slug flow relation (19). For the turbulent liquid case this yields:

$$<\alpha> = \frac{1}{C_o} - <\alpha> \left[\frac{(1-<\alpha>)^2}{B <\alpha>^{2.4}} \phi\right]^{5/9} \quad (33)$$

For the laminar liquid case the model becomes:

$$\left(\frac{1 - C_o <\alpha>}{C_o <\alpha>}\right) U_{GS} = \quad (34)$$

$$\frac{0.00288\ D^{0.8} \nu_G^{0.2} \rho_G U_{GS}^{1.8} (1-<\alpha>)^2 \phi}{\mu_L <\alpha>^{2.4}}$$

The form of ϕ initially chosen is that given by (17). For the case of turbulent liquid, the model (33) predicts that the transition falls along a line of constant void fraction. Solving (33) numerically with the values of C_o determined from Figures 7,8 and 9 yields a transition void fraction of 0.755 for water, 0.741 for water/glycerine and 0.767 for water/Zonyl FSP. Substituting these into (19) results in:

water: $U_{LS} = 0.060\ U_{GS}$ (35)

water/glycerine: $U_{LS} = 0.054\ U_{GS}$ (36)

water/Zonyl FSP: $U_{LS} = 0.051\ U_{GS}$ (37)

The laminar model (34) depends on both <α> and U_{GS} or U_{LS} therefore this transition will not occur along a line of constant void fraction. Equation (34) must be solved numerically.

The locus of points satisfying the turbulent and laminar models represent the predicted transition between slug and annular flow. These are included on the flow maps in Figures 4, 5 and 6. As shown, the models separate the slug-annular transition runs from the annular runs except at the highest values of U_{LS}. If the Wallis model for friction factor (18) is used instead of the experimental measurements, the predicted transitions are shifted slightly into the annular region of the flow maps leading to poorer agreement between the model and the observed flow patterns.

The discrepancy between the transition model and the observed flow patterns may be due to a number of reasons. At high liquid and gas rates, flow pattern identification is difficult at best. At these conditions, the liquid is highly aerated with the slugs and waves traveling at high velocities making identification either by instrumental analysis or photography difficult. The correlation for interfacial stress used in (26) may be subject to considerable error. In addition, recent data indicates that the use of the Blasius equation for f_w will need re-examination.

It should also be noted that the prediction is very sensitive to the value of C_o arrived at from the slug flow data. For example, the second term in (33) influences the value of $<\alpha>$ by less than 10%. Thus using the correct value of C_o is critical.

CONCLUSION

A microgravity two phase flow experiment has been developed to identify the flow patterns present and measure pressure drop, void fraction, liquid film thickness and bubble and wave velocities. From this data, models have been proposed to predict void fraction, bubble and slug velocities, pressure drop and the location of flow patterns transitions on the flow pattern maps. Additional experiments are needed to refine these models.

NOMENCLATURE

A: Cross sectional area of the test section [m^2]
B: Constant defined by equation (31)
C: Blasius equation constant
C_o: Radial void distribution coefficient
D: Test section diameter [m]
F: Any local quantity varying with radial position
f: Fanning friction factor
f_G: Gas phase Fanning friction factor
f_i: Interfacial Fanning friction factor
f_{TP}: Two phase Fanning friction factor
f_w: Wall Fanning friction factor
h: Local liquid film thickness [m]
n: Blasius equation constant
P: Pressure [Pa]
Re: Reynolds number
Re_G: Single phase gas Reynolds number
Re_L: Single phase liquid Reynolds number
Re_{TP}: Two phase mixture Reynolds number
U_G: Local gas velocity [m/s]
U_{GS}: Superficial gas velocity [m/s]
U_L: Local liquid velocity [m/s]
U_{LS}: Superficial liquid velocity [m/s]
U_M: Local volumetric flux [m/s]
U_{MS}: Superficial volumetric flux [m/s]
V_G: Net drift velocity of the gas [m/s]
x: Axial distance along test section [m]

α: Void fraction
ϕ: Annular friction factor enhancement from experiment
μ_L: Liquid viscosity [cP]
ν_G: Gas kinematic viscosity [m^2/s]
ν_L: Liquid kinematic viscosity [m^2/s]
ρ_G: Gas density [kg/m^3]
ρ_L: Liquid density [kg/m^3]
ρ_M: Two phase mixture density [kg/m^3]
σ_L: Liquid surface tension [dyne/cm]
τ_i: Interfacial shear stress [Pa]
τ_w: Wall shear stress [Pa]

REFERENCES

1. Dukler, A.E., Fabre, J. A., McQuillen, J.B. and Vernon, R., "Gas Liquid Flow at Microgravity Conditions: Flow Patterns and Their Transitions", ASME Annual Meeting, Boston, December, 1987.

2. Janicot, A.J.P., M.S. Thesis, University of Houston, 1988.

3. Zuber, N. and Findlay, J.A., "Average Volumetric Concentration in Two-Phase Flow Systems", Journal of Heat Transfer, November, 1965.

4. Wallis, G.B., One Dimensional Two-Phase Flow, McGraw-Hill, New York, 1969.

ACKNOWLEDGMENT

This work was supported by NASA under Grant No. NA 63-510. We wish to especially acknowledge the invaluable assistance of John McQuillen and Eric Neumann at the NASA Lewis Research Center and Robert Mate at the University of Houston.